Int. J. Therm. Sci. (2001) 40, 217–225

S1290-0729(00)01211-4/FLA

Prediction of radial gas profiles in vertical pipe flow on the basis of bubble size distribution

Dirk Lucas *, Eckhard Krepper, Horst-Michael Prasser

Forschungszentrum Rossendorf e.V., Institute of Safety Research, P.O. Box 510 119, D-01314 Dresden, Germany

(Received 13 March 2000, accepted 16 May 2000)

Abstract — A method for the prediction of the radial gas profile for a given bubble size distribution is presented. It is based on the assumption of the equilibrium of the forces acting on a bubble perpendicularly to the flow direction. These forces strongly depend on the bubble size [14, 18]. For the simulation of transient flow regime effects, the modelling of several bubble classes in a 1D model and consideration of their radial profiles seems to be more promising than a detailed 3D modelling. The radial profile of the liquid velocity is calculated by the model of Sato [21, 22]. On the basis of this velocity profile, radial distributions are calculated separately for all bubble classes according to the given bubble size distribution. The sum of these distributions is the radial profile of the gas fraction. It is used in an iteration process to calculate a new velocity profile. There is a strong interaction between the profiles of liquid velocity and gas volume fraction. The model is the basis of a fast running one-dimensional steady state computer code. The results are compared with experimental data obtained for a number of gas and liquid volume flow rates. There is a good agreement between experimental and calculated data. In particular, the change from wall peaking to centre peaking gas fraction distribution is well predicted. © 2001 Éditions scientifiques et médicales Elsevier SAS

two-phase flow / flow pattern / vertical pipe flow / bubble size distribution

Nomenclature

D	diameter of the pipe	m
Eo	Eötvös number	
Eo_d	modified Eötvös number	
F	force per unit volume	$N{\cdot}m^{-3}$
M	Morton number	
R	radius of the pipe	m
Re	Reynolds number	
V	volume	m^3
d	diameter	m
g	constant of gravity acceleration	$9.81\ m{\cdot}s^{-2}$
j	superficial velocity	$m{\cdot}s^{-1}$
k	turbulent kinetic energy	$m^2{\cdot}s^{-2}$
n	bubble density	m^{-3}
r	radius	m
t	time	s
w	velocity	$m{\cdot}s^{-1}$
y	distance from the wall	m

Greek symbols

α	gas volume fraction	
ε	energy dissipation rate per unit mass	$m^2{\cdot}s^{-3}$
μ	viscosity	$N{\cdot}s{\cdot}m^{-2}$
ρ	density	$kg{\cdot}m^{-3}$
σ	surface tension	$N{\cdot}m^{-1}$
τ	shear stress	$N{\cdot}m^{-2}$

Indices

D	refers to the dispersion force
D, *Eo*	refers to the Eötvös-number-dependent dispersion force
H	horizontal
L	refers to the lift force
T	refers to the net transverse lift force
W	refers to the wall force
bubb	property of a bubble
g	gas phase
i	number of the bubble class
l	liquid phase
rel	relative
t	turbulent
w	wall

* Correspondence and reprints.

E-mail addresses: lucas@fz-rossendorf.de (D. Lucas), krepper@fz-rossendorf.de (E. Krepper), prasser@fz-rossendorf.de (H.-M. Prasser).

1. INTRODUCTION

The knowledge of the flow pattern is essential for one-dimensional models of two-phase pipe flows. Such models are frequently used for practical applications in the field of design, optimisation and safety analysis of chemical and nuclear plants. Most of the correlations used by these codes, e.g., for pressure drop or heat and mass transfer, are valid only for a given flow regime. For the prediction of the flow regime, empirical and theoretical flow pattern maps have been developed (see, e.g., [1]). In general, the flow pattern may change along the flow path as well as with time. However, only steady state flow maps for fully developed flow conditions are state of the art. They are not able to predict the transient restructuring of the flow pattern. Recently attempts were made to solve this problem by the introduction of additional equations for the bubble density or corresponding parameters like bubble diameter, bubble volume or interfacial area (see, e.g., [2]). Such models have to consider bubble coalescence and bubble break-up.

In literature several models are available for bubble coalescence and break-up [3–5]. The rates for both processes depend on the bubble density. If an equation for the particle density or any equivalent parameter is included in one-dimensional models this parameter is formally available, but averaged over an area perpendicular to the flow path.

Many investigations were done concerning the radial gas profiles in vertical pipe flow [6–9]. In some cases wall peaking was observed in other cases a peak in the pipe centre was found. The gas profiles are the result of the nondrag forces, acting perpendicularly to the flow direction, which are caused by the liquid shear flow in the tube. Zun derived a lift force, to which a spherical obstacle in a shear flow is subjected [10]. According to the liquid velocity profile, found in a vertical tube upwards flow, this lift force acts into wall direction. Antal et al. [11] proposed to consider in addition a lubrication force, which acts to drive the bubbles away from the wall. Tomiyama et al. [12, 13] proposed an extended definition of the lift force, changing its sign depending on the bubble diameter. In case of a water–air system under atmospheric pressure this change was found at a bubble diameter of about 5.8 mm. Bubbles with a diameter below 5.8 mm should be found preferably near the wall and larger bubbles in the pipe centre.

This fact is very important for the modelling of the spatial evolution of developing two-phase bubble flow in a vertical pipe including the prediction of a change of the flow pattern. Bubble coalescence and break-up must be understood as local events. Their rates depend on the local quantities of the bubble number densities and bubble sizes. For this reason the total rates over the pipe cross section are controlled by the radial distributions of the bubbles depending on their size. To give an example, the coalescence rate for 3 mm bubbles with 8 mm bubbles should be much smaller in case of consideration of the radial distributions compared to a model that uses particle densities averaged over the pipe cross section. The 3 mm bubbles are located preferably in the wall region and the 8 mm bubbles near to the pipe centre. This means, collisions between a 3 mm bubble and an 8 mm bubble are less likely than predicted considering uniform radial distributions.

The collision between a bubble and an eddy is assumed to be the reason for bubble fragmentation (see, e.g., [5]). Because of the larger shear stress, the collision frequency between a bubble and an eddy in the wall region is larger than in the centre. That means for a bubble with a given diameter the break-up rate is larger in wall region. A bubble with a diameter larger than 5.8 mm, generated in wall region by coalescence of two smaller bubbles, migrates to the pipe centre. If it is stable enough to do this migration without break-up, it has a good chance to survive also in the pipe centre. For this reason the appearance of relatively stable bubbles larger than 5.8 mm (air–water system) is a necessary condition for the change from bubble to slug flow.

That means:

(1) The consideration of the bubble size distribution is essential for the prediction of the change of the flow pattern.

(2) The radial gas fraction distribution must be resolved into the contributions of bubbles according to their size for calculating rates for coalescence and break-up.

Many attempts were done to use two- or three-dimensional CFD codes to predict radial distributions of the gas fraction [8, 14, 15]. Because of the high computational effort there are limits in considering several bubble classes in multi-dimensional calculations. The ideas discussed above suggest that for a first step the consideration of the bubble size distribution should be more important for evolution of the flow than a transient modelling of three-dimensional velocity fields.

A one-dimensional model was developed, which resolves the parameters in radial direction. It allows the prediction of the radial bubble distributions in a vertical pipe flow from a given bubble size distribution. Experimentally determined bubble size distributions were used as input of the model. They were measured for several combinations of gas and liquid volume flow rates. The model

is based on the assumption of equilibrium of the forces acting on a bubble perpendicularly to the main flow direction, what corresponds to fully established profiles. This quasi-stationary approach leads to low computational efforts. By this model the dependence of radial distributions on the bubble diameter can be checked using a large number of bubble classes.

2. THE MODEL

2.1. Balance of the forces acting perpendicularly to the flow direction

In vertical pipe flow, forces acting perpendicularly to the flow direction (nondrag forces) determine the establishment of radial gas profiles or, in other words, radial distributions of the bubbles. The forces taken into account are: the transverse lift force, the lubrication or wall force and dispersion forces. The model does not consider single bubbles, but the radial distributions of volume fractions. For a mono-dispersed flow with bubbles with a volume V_{bubb} the volume fraction can be defined as

$$\alpha = V_{\mathrm{bubb}} n_{\mathrm{bubb}} \tag{1}$$

where n_{bubb} is the number of bubbles per unit volume.

According to [16, 17] the forces acting on a bubble are determined by the Reynolds number, Eötvös number and Morton number:

$$Re = \frac{\rho_{\mathrm{l}} w_{\mathrm{rel}} d_{\mathrm{bubb}}}{\mu_{\mathrm{l}}} \tag{2}$$

$$Eo = \frac{g(\rho_{\mathrm{l}} - \rho_{\mathrm{g}}) d_{\mathrm{bubb}}^2}{\sigma} \tag{3}$$

$$M = \frac{g \mu_{\mathrm{l}}^4 (\rho_{\mathrm{l}} - \rho_{\mathrm{g}})}{\rho_{\mathrm{l}} \sigma^3} \tag{4}$$

The classical *lift force* was introduced about 20 years ago to model the observed wall peaking [10]. This force is shear induced. Related to the unit volume it can be calculated as

$$\boldsymbol{F}_{\mathrm{L}} = -C_{\mathrm{L}} \rho_{\mathrm{l}} (\boldsymbol{w}_{\mathrm{g}} - \boldsymbol{w}_{\mathrm{l}}) \times \mathrm{rot}(\boldsymbol{w}_{\mathrm{l}}) \tag{5}$$

with a positive lift force coefficient C_{L}. A positive sign means that the lift force acts towards decreasing liquid velocity, i.e. for the upwards flow in a vertical pipe towards the pipe wall. Tomiyama et al. [12] proposed another kind of transverse lift force, which is caused by the interaction between the wake and the shear field. It acts in the opposite direction, that means it is also calculated by equation (5), but has a negative coefficient C_{L}. Tomiyama et al. [18] express both forces summarized as a net transverse lift force with the experimentally determined coefficient C_{T}:

$$C_{\mathrm{T}} = \begin{cases} \min\left[0.288 \tanh(0.121 Re),\, f(Eo_{\mathrm{d}})\right] \\ \quad \text{for } Eo_{\mathrm{d}} < 4 \\ f(Eo_{\mathrm{d}}) \quad \text{for } 4 < Eo_{\mathrm{d}} < 10 \\ 0.29 \quad \text{for } Eo_{\mathrm{d}} > 10 \end{cases} \tag{6}$$

with

$$f(Eo_{\mathrm{d}}) = 0.00105 Eo_{\mathrm{d}}^3 - 0.0159 Eo_{\mathrm{d}}^2 - 0.0204 Eo_{\mathrm{d}} + 0.474$$

This coefficient depends on the modified Eötvös number given by

$$Eo_{\mathrm{d}} = \frac{g(\rho_{\mathrm{l}} - \rho_{\mathrm{g}}) d_{\mathrm{H}}^2}{\sigma} \tag{7}$$

Here d_{H} is the maximum horizontal dimension of the bubble. It is calculated using an empirical correlation for the aspect ratio from [19] by the following equation:

$$d_{\mathrm{H}} = d_{\mathrm{bubb}} \sqrt[3]{1 + 0.163 Eo^{0.757}} \tag{8}$$

For the water–air system at normal conditions C_{T} changes its sign at $d_{\mathrm{bubb}} = 5.8$ mm.

The *lubrication force*, introduced by Antal et al. [11], acts to drive bubbles away from the wall. Tomiyama et al. [12] developed a modified equation for this force per unit volume:

$$\boldsymbol{F}_{\mathrm{W}} = -C_{\mathrm{W}} \frac{d_{\mathrm{bubb}}}{2} \left(\frac{1}{y^2} - \frac{1}{(D-y)^2} \right) \rho_{\mathrm{l}} w_{\mathrm{rel}}^2 \boldsymbol{n}_{\mathrm{r}} \tag{9}$$

They determined the coefficient C_{W} for a system with $\log M = -2.8$ as

$$C_{\mathrm{W}} = \begin{cases} \exp(-0.933 Eo + 0.179) & \text{for } 1 \le Eo \le 5 \\ 0.007 Eo + 0.04 & \text{for } 5 \le Eo \le 33 \end{cases} \tag{10}$$

As mentioned above, the presented model does not consider individual bubbles, but continuous radial distributions. The *turbulent dispersion force* considers the smoothing of these radial gas profiles caused by the turbulence. That means, this force is introduced to simulate a phasic diffusion. Lahey et al. [20] derived an equation for the force per unit volume as

$$\boldsymbol{F}_{\mathrm{D}} = -0.1 \rho_{\mathrm{l}} k_{\mathrm{l}} \,\mathrm{grad}\alpha \tag{11}$$

Following [14] there is a fluctuating motion of single bubbles, which increases with the Eötvös number. It

is caused by the deformation of the bubbles. These fluctuations cause an additional smoothing of the profiles, which is not covered by the dispersion force according to equation (11). For this reason a second dispersion force is introduced, which depends on the Eötvös number. As reported in [14] the fluctuations were observed at bubbles with Eötvös numbers larger than about 1. For this reason we stated

$$\boldsymbol{F}_{\mathrm{D},Eo} = -C_{\mathrm{D},Eo}\rho_{\mathrm{l}}(Eo-1)\mathrm{grad}\alpha \tag{12}$$

The parameter $C_{\mathrm{D},Eo}$ is the only new model parameter. According to integral experimental data (see below) $C_{\mathrm{D},Eo} = 0.0015\ \mathrm{m^2{\cdot}s^{-2}}$ is assumed for $Eo > 1$. For $Eo < 1$ $C_{\mathrm{D},Eo}$ is set to zero.

The radial balance of forces can be written as

$$\alpha_i(F_{\mathrm{L}} + F_{\mathrm{W}}) + F_{\mathrm{D}} + F_{\mathrm{D},Eo} = 0 \tag{13}$$

where the scalar forces denote the components in radial direction. Applying equations (5), (9), (11) and (12) the resulting equation is

$$\left(0.1k_{\mathrm{l}} + C_{\mathrm{D},Eo}(Eo-1)\right)\frac{\mathrm{d}\alpha}{\mathrm{d}r} + \left(C_{\mathrm{T}}w_{\mathrm{rel}}\frac{\mathrm{d}w_{\mathrm{l}}}{\mathrm{d}r} + C_{\mathrm{W}}\frac{d_{\mathrm{bubb}}}{2}\left(\frac{1}{(R-r)^2} - \frac{1}{(R+r)^2}\right)w_{\mathrm{rel}}^2\right)\alpha = 0 \tag{14}$$

This equation is a first-order differential equation with respect to $\alpha(r)$. The coefficients depend on r. The equation is valid only for a mono-dispersed bubble distribution with a bubble diameter d_{bubb}.

For real bubble distributions a subdivision into several bubble classes is done. According to these bubble classes the gas volume fraction α is subdivided into gas volume fractions α_i with

$$\alpha(r) = \sum_i \alpha_i(r) \tag{15}$$

α_i is the total volume fraction of bubbles with a diameter, which is within the bubble class i. Equation (14) has now to be solved separately for each bubble class i with $\alpha_i(r)$ as a result. For given coefficients it is solved starting at the centre of the pipe with $\alpha_i(r=0) = 1$. The resulting $\alpha_i(r)$ is renormalized according to the volume fraction of the bubble class i in the bubble size distribution.

The coefficients in equation (14) depend on the turbulent kinetic energy of the liquid k_{l} and the gradient of the liquid velocity $\mathrm{d}w_{\mathrm{l}}/\mathrm{d}r$ as a function of the radius. Their calculation is presented in the next two chapters. They depend on $\alpha(r)$, and so the system of equations is solved by an iteration procedure. The dependence of the relative velocity of the gas phase compared to the liquid w_{rel} on the radial position is neglected, but an average value for each bubble class is calculated using the drag coefficient given in [14].

2.2. Radial profile of the liquid velocity

The radial profile of the liquid velocity is calculated for a given radial gas distribution using the model of Sato et al. [21, 22]. They subdivided the eddy diffusivity into two components. The first component considers the inherent wall turbulence, which does not depend on the bubble agitation, the second considers the turbulence caused by the bubbles. This causes a feedback between the radial gas profile and the radial profile of liquid velocity. The complete model equations as well as a scheme for a numerical solution procedure can be found in [22]. The wall shear stress τ_{w} is calculated by an iteration procedure until the averaged liquid velocity equals to the given liquid volume flow rate.

Besides the radial gas profile $\alpha(r)$ the model of Sato needs as an input the bubble diameter and the relative velocity of the gas w_{rel}. For the last two parameters values averaged over all bubble classes are taken to keep the model simple. In the result the radial profile of the liquid velocity $\mathrm{d}w_{\mathrm{l}}/\mathrm{d}r$ and the turbulent viscosity μ_{t} are calculated as functions of the radius.

2.3. Radial profile of the liquid turbulent kinetic energy

For the calculation of the turbulent kinetic energy the equations of the k–ε model are used. A common nonlinear differential equation of the second order for the steady state turbulent kinetic energy k of the liquid can be derived by using the following assumptions:

- The time-averaged liquid velocity has only a component in axial direction.
- The time-averaged liquid velocity is only a function of the radius and does not depend on the azimuthal position and the height.

According to the k–ε model, the turbulent energy k satisfies the following balance equation:

$$\frac{\partial}{\partial t}\rho_{\mathrm{l}}k_{\mathrm{l}} + \mathrm{div}(\rho_{\mathrm{l}}k_{\mathrm{l}}\boldsymbol{w}_{\mathrm{l}}) = \mathrm{div}\left(\frac{\mu_{\mathrm{t}}}{\sigma_{\mathrm{k}}}\mathrm{grad}(k_{\mathrm{l}})\right) + P_k - \rho_{\mathrm{l}}\varepsilon \tag{16}$$

with the turbulence production term P_k, which simplifies with the assumptions mentioned above to

$$P_k = \mu_t \left(\frac{dw_l}{dr} \right)^2 \tag{17}$$

Further, the relation

$$\mu_t = C_\mu \rho_l \frac{k^2}{\varepsilon} \tag{18}$$

is used.

For steady state conditions and considering only radial dependences of all properties and the relations (17) and (18) the equation (16) results in

$$\frac{\mu_t}{\sigma_k} \frac{d^2 k_l}{dr^2} + \left(\frac{1}{\sigma_k} \frac{d\mu_t}{dr} + \frac{\mu_t}{\sigma_k} \frac{1}{r} \right) \frac{dk_l}{dr} - \frac{C_\mu \rho_l^2}{\mu_t} k_l^2 + \mu_t \left(\frac{dw_l}{dr} \right)^2 = 0 \tag{19}$$

This equation is transferred to a discrete difference scheme and solved with the boundary conditions $k_l(R) = 0$ and $dk_l/dr = 0$ for $r = 0$.

2.4. Iteration procedure

The radial gas fraction profiles are calculated by an iterative procedure. The iteration starts from a uniform distribution of the gas fraction. The radial profile of liquid velocity and afterwards the radial profile of the liquid turbulent energy are calculated for this gas profile. Then equation (14) is solved for each bubble class. $\alpha(r)$ is calculated according to equation (15). This is used for a new calculation of radial profiles of liquid velocity and turbulent kinetic energy. An under-relaxation is necessary to guarantee the stability of the iteration.

There is a very sensitive feedback between the velocity profile and the gas fraction profile. In case of a flow with bubble sizes below 5.8 mm the feedback smoothes the radial gas profiles. The bubbles are located preferably at the wall region. For this reason the liquid velocity near the wall is increased. This smoothes the velocity profile apart from the wall and reduces the lift force in the core region of the flow, which acts towards the wall.

Otherwise, if a considerable fraction of bubbles with a diameter larger than 5.8 mm occurs, there is a positive feedback between the gas and velocity profiles. The bubbles in the centre accelerate the liquid. For this reason the velocity gradient in the central region increases. This again causes an increase of the lift force, which acts towards the pipe centre. The turbulent component of the dispersion force is not large enough to distribute the large bubble over the cross section of the pipe. Instead they accumulate near the centreline, which is in contradiction to the experimental observations. Obviously, another mechanism is dispersing the bubbles, which is not covered by any of the models introduced up to now. The fluctuating movement of the large bubbles, as observed by Tomiyama [14], may be such a mechanism. Due to the oscillatory trajectory, the bubbles are moved away from the centreline. That is why the additional dispersion force according to equation (12) was introduced. It describes the fluctuating movement of large bubbles and prevents their accumulation within a small region close to the centreline. The parameter $C_{D,Eo}$ was tuned to achieve a good agreement between calculated and measured radial profiles for large bubbles.

Besides the description of fluctuations in bubble motion, this additional dispersion force also solves two other problems of the model. At first the balance of forces is based on the assumption of an idealised bubble, where all forces act at the centre of mass. In reality, the bubble is exposed to an inhomogeneous liquid velocity profile and the forces act on the bubble surface. The larger the bubble diameter the more the velocity gradient over the bubble differs from that at the centre of mass. This is especially important if the bubble is located near the maximum of the velocity profile. In this case the real lift force is hard to determine, because the force calculated for the location of the centre of mass differs significantly from the forces acting at the bubble surface, which may even act in different directions. The second problem is that the velocity profile is distorted by large single bubbles. For this reason it can be assumed that the calculated lift force is not consistent if the bubble diameter is larger than about half of pipe diameter. These problems are partially compensated by the Eötvös-number-dependent dispersion force.

Calculations with an assumed velocity profile according to a $1/m$ law have shown that the feedback of the gas fraction profile on the velocity profile is not negligible. Even for an integral gas fraction of only 1–2 % the gas fraction profiles calculated by the presented model differ significantly from that obtained with a constant velocity profile.

3. COMPARISON WITH EXPERIMENTAL DATA

Experimental data obtained from measurements at the two-phase flow test loop of the Institute of Safety

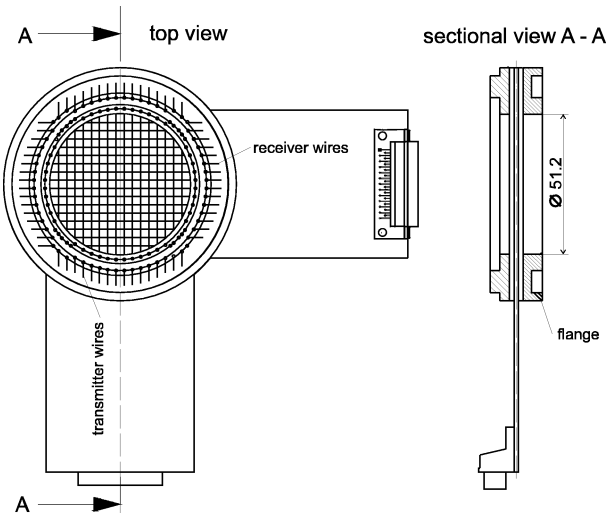

Figure 1. Scheme of the wire mesh sensor with 16×16 electrode wires.

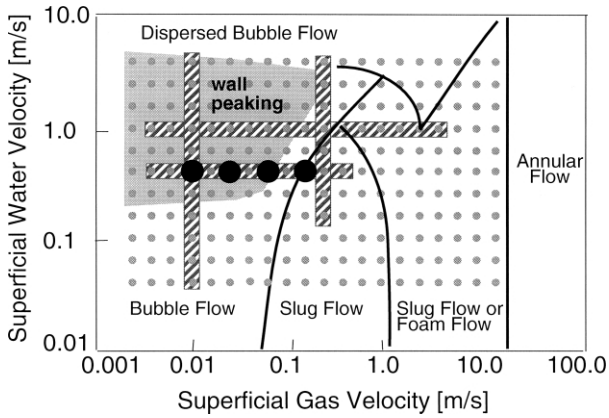

Figure 2. Flow map. The borderlines for the transition of the flow regimes were taken from [1]. The points indicate the performed tests. The marked points were used for the validation of the model.

Research [23] were used for the validation of the model. The measurements were carried out at a vertical test section of 4 m height and 51.2 mm inner diameter. Water–air flow under normal conditions was used. Air was injected through a system of capillaries. The ends of these capillaries are equally distributed over the cross section of the pipe. During one experiment gas and liquid flow rates were held at constant values, i.e. the properties of the flow changed only with the distance along the pipe, but were constant in time.

The test section was equipped with a wire mesh sensor [24], shown in *figure 1*. The sensor consists of two layers, each of 16 parallel wires with a distance of 3 mm. The two layers are arranged with crossed wires. The distance between the layers amounts to 1.5 mm. By a multiplex electronic circuit the conductivity is measured subsequently at each cross point. On the basis of the local instantaneous conductivity of the two-phase mixture at the crossing points of the wires of the two grids, the sensor allows the determination of the gas fraction distribution over the area of the sensor with a frequency of 1 200 frames per second. The wire-mesh sensor delivers a sequence of two-dimensional distributions of the local instantaneous gas fraction $\varepsilon(i, j, k)$, measured in each mesh formed by two crossing electrodes. Here i is the number of the transmitter wire, j the receiver wire. The index k denominates the instantaneous current distribution in time. In general, a bubble is extended over more than one mesh. Due to the high time resolution it is mostly mapped in several successive frames. By integrating the local instantaneous gas fractions over the area belonging to a bubble, its volume and, consequently, its effective diameter can be assessed. This allows one to obtain bubble size distributions [23, 25]. This requires the following steps of data processing:

- Identification of bubbles, i.e. of areas containing gas and surrounded by the liquid phase. Technically this is done by assigning an identifying number to all elements (i, j, k) of the measured gas fraction distribution $\varepsilon(i, j, k)$ that fulfils the mentioned condition.
- Integrating the local instantaneous gas fraction over the elements belonging to the given bubble to obtain the bubble volume and transfer to an equivalent diameter.
- Calculation of a statistical distribution with the equivalent bubble diameter as variable.

Two-dimensional gas fraction profiles can be obtained by averaging the instantaneous two-dimensional distributions over a period of several seconds. Using the identifying number that indicates to which bubble a given local instantaneous gas fraction value belongs, profiles can be calculated also considering only those bubbles, the diameter of which lies in a given interval. This results in partial gas fraction profiles for a distinct bubble size interval.

Measurements were performed for a large number of combinations of liquid and gas volume flow rates at 7 different height positions. For the validation of the presented model the upper position ($L/D = 60$) and the combinations of volume flow rates marked in *figure 2* by the bars were used. Measured bubble size distributions were used as an input of the model. The width of the bubble classes was 0.25 mm.

The model well predicted wall or centre peaking of the gas volume fraction for all the investigated data points. As an example, *figures 3–6* show the radial profiles for

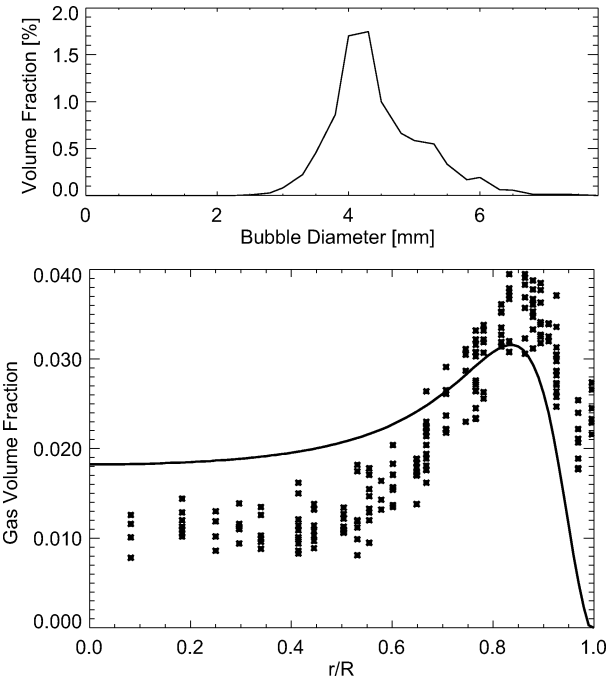

Figure 3. Measured bubble size distribution and radial gas distribution (solid line: prediction, stars: experimental data), $j_l = 0.4048$ m·s^{-1}, $j_g = 0.0096$ m·s^{-1}.

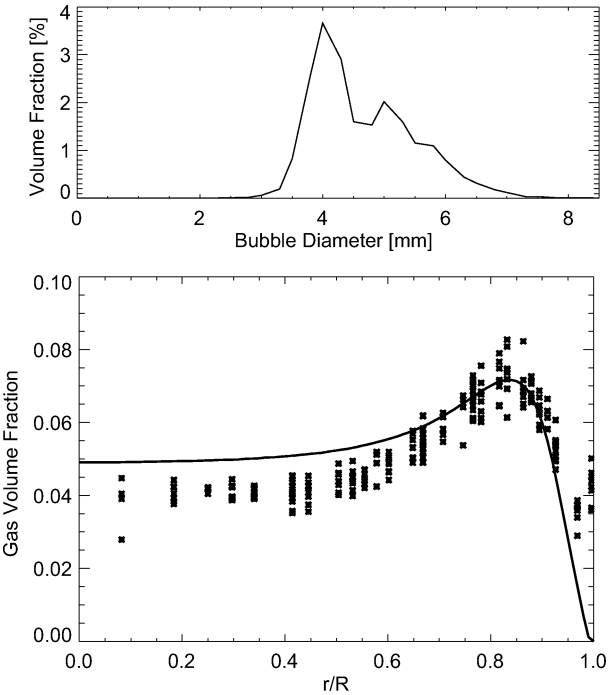

Figure 4. Measured bubble size distribution and radial gas distribution (solid line: prediction, stars: experimental data), $j_l = 0.4048$ m·s^{-1}, $j_g = 0.0235$ m·s^{-1}.

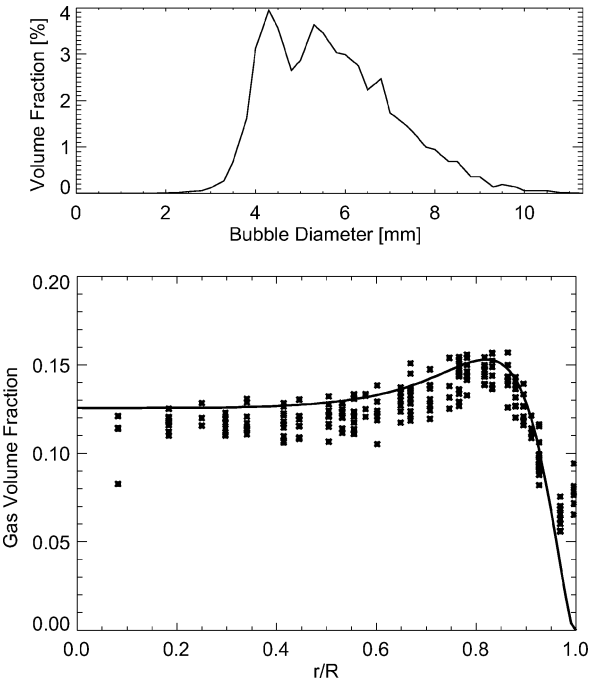

Figure 5. Measured bubble size distribution and radial gas distribution (solid line: prediction, stars: experimental data), $j_l = 0.4048$ m·s^{-1}, $j_g = 0.0574$ m·s^{-1}.

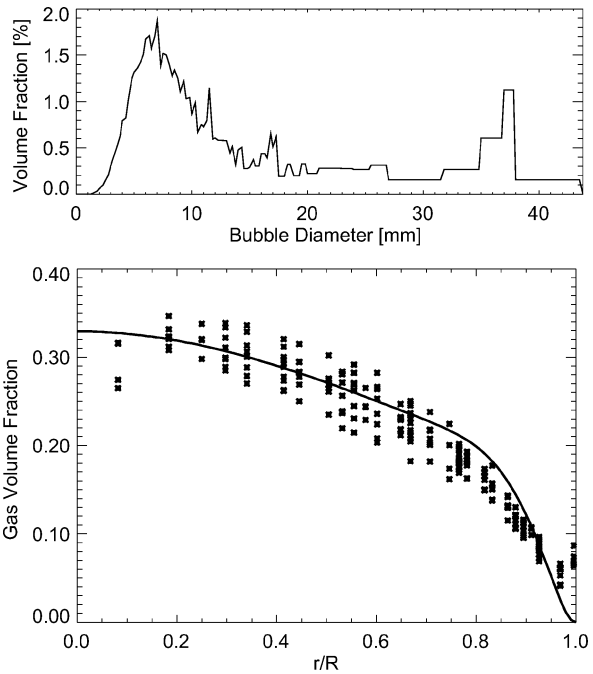

Figure 6. Measured bubble size distribution and radial gas distribution (solid line: prediction, stars: experimental data), $j_l = 0.4048$ m·s^{-1}, $j_g = 0.1402$ m·s^{-1}.

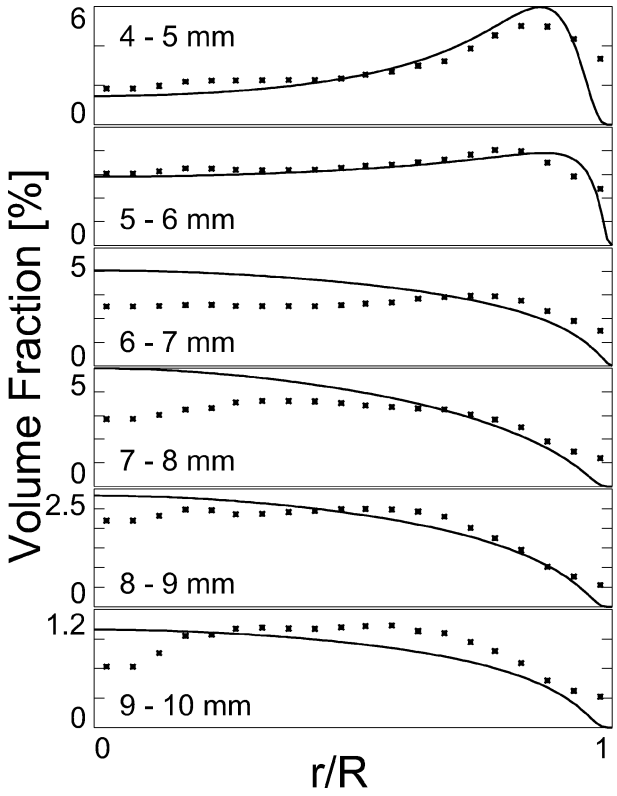

Figure 7. Measured (stars) and predicted (solid line) radial profiles of the gas fraction in dependence on the bubble diameter.

the 4 bold marked points of the flowmap (see *figure 2*). The liquid superficial velocity equals to 0.4048 $m{\cdot}s^{-1}$ and the gas superficial velocity increases from 0.0096 to 0.1402 $m{\cdot}s^{-1}$. The experimental data are plotted for each crossing point of the wires of the two grids (see *figure 1*). For this reason, several data points are plotted for one radial position. The scattering of them is caused by some azimuthal non-uniformity. The radial profiles are very well predicted by the model. Please note that the coefficient for the Eötvös-number-dependent dispersion force is the only tuned parameter of the model! All other parameters were taken from literature without any change.

Figure 7 shows a comparison of the radial profiles of the gas fraction for distinct bubble size classes for $j_l = 0.4048\ m{\cdot}s^{-1}$ and $j_g = 0.0574\ m{\cdot}s^{-1}$. There is a very good agreement between calculated and measured data. This confirms the results from [14] concerning the bubble size or Eötvös number dependence of the lift force and radial gas fraction profiles.

The largest deviations of measured and predicted profiles were found in the transition region from wall peaking to centre peaking (see *figure 2*). In some cases the profiles are overestimated in the centre region. This may be explained by the limitation of the model to steady state conditions. In reality in such cases there is a high coalescence rate for bubbles below 5.8 mm in the near-wall region. Due to the coalescence, bubbles larger than 5.8 mm are generated. However, the model assumes an equilibrium of the radial forces, that means these bubbles immediately move to the centre region. In reality they need some time to move from the wall region to the centre. Therefore, they are found still near the wall in the experimental data. This also explains the overestimation of the gas fraction in the pipe centre in the case of 6–8 mm bubbles shown in *figure 7*.

4. CONCLUSIONS

The presented model allows the prediction of radial gas profiles in vertical pipe flows. In particular, the model allows a prediction whether wall peaking or centre peaking occurs in dependence on the gas and liquid volume flow rates and the bubble size distribution. The good agreement between experimental and calculated data confirms the dependence of the radial forces acting on a bubble on the bubble size as reported by Tomiyama [14]. The correlations for these forces as well as the model for the radial velocity profile form were taken from literature without any change of the empirical parameters. The only extension was the introduction of Eötvös-number-dependent dispersion force.

The dependence of radial forces on bubble size is very important for the modelling of the transition between bubble flow and slug flow. It is supposed that the attempts for a one-dimensional modelling of bubble coalescence and bubble break-up suffer from neglecting the radial profiles of the particle densities for the single bubble classes.

This assumption will be proved in a next step by including correlations for bubble coalescence and break-up into the presented model. Then only an initial bubble size distribution has to be given and the change of this distribution in time can be evaluated. That corresponds to the change of a bubble size distribution along the flow path, if the differences of the velocity of different bubble classes are neglected. Another possibility is a connection of this model with a one-way bubble tracking method as suggested in [18].

REFERENCES

[1] Taitel Y., Bornea D., Duckler A.E., Modelling flow pattern transitions for steady upward gas-liquid flow in vertical tubes, AIChE J. 26 (1980) 345–354.

[2] Milles M., Mewes D., Phasengrenzflächen in Blasenströmungen — Teil 1, Blasensäulen, Chemie Ingenieur Technik 68 (1996) 660–669.

[3] Prince M.-J., Blanch H.W., Bubble coalescence and break-up in air-sparged bubble columns, AIChE J. 36 (1990) 1485–1499.

[4] Das R.K., Pattanayak S., Bubble to slug flow transition in vertical upward two-phase flow through narrow tubes, Chem. Engrg. Sci. 49 (1994) 2163–2172.

[5] Luo H., Svendsen H.F., Theoretical model for drop and bubble breakup in turbulent dispersions, AIChE J. 42 (1996) 1225–1233.

[6] Hibiki T., Ishii M., Experimental study on interfacial area transport in bubbly two-phase flows, Int. J. Heat Mass Tran. 42 (1990) 3019–3035.

[7] Kataoka I., Serizawa A., Interfacial area concentration in bubbly flow, Nuclear Engineering and Design 120 (1990) 163–180.

[8] Krepper E., Prasser H.-M., Measurements and CFX-simulations of a bubbly flow in a vertical pipe, in: CFX International Users Conference, Friedrichshafen, Germany, June, 1999.

[9] Sengpiel W., Samstag M., Heinzel V., Simon M., Messungen der Eigenschaften von kontinuierlicher und disperser Phase in Luft-Wasser-Blasenströmungen, in: 3. Workshop "Meßtechnik für stationäre und transiente Mehrphasenströmungen", 14 October 1999, Rossendorf, FZR-281, pp. 25–49.

[10] Zun I., The transverse migration of bubbles influenced by walls in vertical bubbly flow, Int. J. Multiphase Flow 6 (1980) 583–588.

[11] Antal S.P., Lahey R.T., Flaherty J.E., Analysis of phase distribution in fully developed laminar bubbly two-phase flow, Int. J. Multiphase Flow 7 (1991) 635–652.

[12] Tomiyama A., Sou A., Zun I., Kanami N., Sakaguchi T., Effects of Eötvös number and dimensionless liquid volumetric flux on lateral motion of a bubble in a laminar duct flow, in: Advances in Multiphase Flow, 1995, pp. 3–15.

[13] Tomiyama A., Zun I., Tamai H., Hosokawa S., Okuda T., Measurement of transverse migration of single bubbles in a couette flow, in: Proc. 2nd Int. Symp. on Two-phase Flow Modelling and Experimentation, Vol. II, Pisa, 1999, pp. 941–948.

[14] Tomiyama A., Struggle with computational bubble dynamics, in: Third International Conference on Multiphase Flow, ICMF '98, Lyon, France, June 8–12, 1998.

[15] Lance M., Lopez de Bertodano M., Phase distribution phenomena and wall effects in bubbly two-phase flows, Multiphase Science and Technology 8 (1994) 69–123.

[16] Bhaga D., Weber M.E., In-line interaction of a pair of bubbles in a viscous liquid, Chem. Engrg. Sci. 35 (1980) 2467–2474.

[17] Bhaga D., Weber M.E., Bubbles in viscous liquids: shapes, wakes and velocities, J. Fluid Mech. 105 (1981) 61–85.

[18] Tomiyama A., Tamai H., Shimomura H., Hosokawa S., Spatial evolution of developing air-water bubble flow in a vertical pipe, in: Proc. 2nd Int. Symp. on Two-phase Flow Modelling and Experimentation, Vol II, Pisa, 1999, pp. 1027–1034.

[19] Wellek R.M., Agrawal A.K., Skelland A.H.P., Shapes of liquid drops moving in liquid media, AIChE J. 12 (1966) 854.

[20] Lahey R.T., Lopez de Bertodano M., Jones O.C., Phase distribution in complex geometry conduits, Nuclear Engineering and Design 141 (1993) 177–201.

[21] Sato Y., Sekoguchi K., Liquid velocity distribution in two phase bubble flow, Int. J. Multiphase Flow 2 (1975) 79.

[22] Sato Y., Sadatomi M., Sekoguchi K., Momentum and heat transfer in two-phase bubble flow I, Int. J. Multiphase Flow 7 (1981) 167–177.

[23] Krepper E., Krüssenberg A.-K., Prasser H.-M., Schaffrath A., High resolution measurements for the validation of flow maps and CFD codes, in: Proc. 2nd International Symposium on Two-phase Flow Modelling and Experimentation, Vol. III, Pisa, 1999, pp. 1371–1378.

[24] Prasser H.-M., Böttger A., Zschau J., A new electrode-mesh tomograph for gas-liquid flows, Flow Measurement and Instrumentation 9 (1998) 111–119.

[25] Prasser H.-M., Messung von Blasengrössenverteilungen mit Gittersensoren, 2. Workshop "Meßtechnik für stationäre und transiente Mehrphasenströmungen", 24–25 September 1998, Rossendorf, FZR-241, pp. 157–164.